Ninth International Conference on CFD in the Minerals and Process Industries
CSIRO, Melbourne, Australia
10-12 December 2012

COUPLED CFD-PBE SIMULATION FOR NUCLEATION AND PARTICLE GROWTH IN FLUIDIZED BED SPRAY GRANULATION

Zhen. LI[1], Jasmina. KESSEL[2], Gerald. GRÜNEWALD[2], Matthias. KIND[1]*

[1] Karlsruhe Institute of Technology (KIT), Thermische Verfahrenstechnik D-76131, Karlsruhe, Germany
[2] BASF SE, D-67056 Ludwigshafen, Germany
*Corresponding author, E-mail address: matthias.kind@kit.edu

ABSTRACT

Fluidized bed spray granulation is used to produce porous granular particles from suspensions, solutions and melts. It is the general aim of our work to provide a physics-based simulation tool for this process. For this the process relevant mechanisms like e.g. drop deposition, dust integration and drying are implemented in CFD to generate growth kinetics of the granules and of the dust particles. The latter gives rise to the nucleation rate. This kinetics is applied to simulate the development of the particle size distribution of granules for a continuously operated fluidized bed spray granulation process using population balance equations of the granules.

NOMENCLATURE

d	diameter	m
G_L	length based growth rate	ms^{-1}
G_V	volume based growth rate	m^3s^{-1}
L	abscissa	m
$n(L)$	particle size distribution	m^{-1}
N	number	-
$\dot{N}$	number flow	s^{-1}
N_{conc}	number concentration	m^{-3}
m_k	kth moment	m^k
$\dot{m}$	mass stream	kgs^{-1}
$\bar{S}_k$	source of the k-th moment	m^ks^{-1}
u	velocity	ms^{-1}
w	weight	-
x	weight percent	-
α	volume fraction	-
β	collision rate	m^3s^{-1}
β_{total}	total agglomeration rate	ms^{-1}
ε	turbulence energy dissipation	m^2s^{-3}
ν	kinematical viscosity	m^2s^{-1}
τ	relaxation time	s
ρ	density	kgm^{-3}

INTRODUCTION

Fluidized bed spray granulation is used to produce porous granular particles from suspensions, solutions and melts. Specific particle size or particle size distributions (PSD) are required according to the different applications of the produced granules. Thus, the ability to predict the development of the PSD is crucial for process design. For this purpose a population balance approach can be used. However the formulation for the population balance equation (PBE) requires the knowledge about growth and nucleation kinetics, which are not easily accessible by experiments. For short process times (several seconds) these kinetics can be obtained with the help of computational fluid dynamics (CFD) from a detailed and local resolution of the process. Applying these kinetics to PBE allows to simulate the evolution of the PSD for long process times (several hours). For describing spray granulation processes three principal mechanisms of drop deposition, drying and dust integration have to be considered. In the process shown in Figure 1 the liquid feed is atomized to droplets by a nozzle and the droplets are injected into the fluidized bed. Some of them are deposited on the surface of the granules and form a film which is dried to build a solidified layer. This growth mechanism is called drop deposition. The drops, which do not deposit on the granules, are dried to primary dust, which is separated from the exhaust by a filter and fed back into the process. These dust particles can deposit and adhere on the surface of wet granules. This growth mechanism is called dust integration.

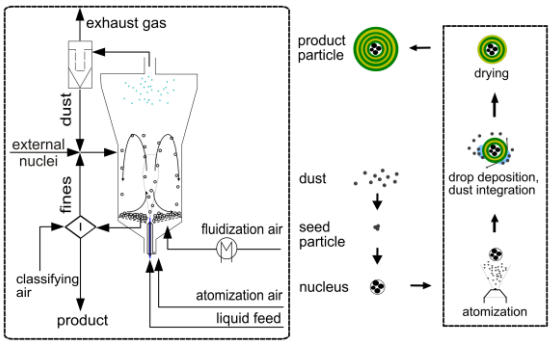

Figure 1: Process scheme

Furthermore, dust particles and droplets can collide and thus let the dust particles grow. They can also grow due to collisions among themselves. These secondary grown dust particles are not withheld in the fluidized bed, but are collected in the filter and from there are returned to the bed. However, after many circulations some of the secondary dust particles become nuclei, which are large enough to stay in the fluidized bed. Thus the dust particles have a PSD from primary dust particle size to nuclei size. External nuclei may be added to the granulator.

EXPERIMENTAL CONDITIONS

Results of numerical simulation calculations are compared to experiments carried out by Grünewald (2011). In these experiments a two-fluid nozzle in bottom-spray

configuration is positioned central in the circular fluidized bed of 23 cm diameter. The elutriated dust particles are separated from the exhaust air by four pulse-jet cleaned bag filters and are collected in a hopper. Every 30 seconds one of the four bag filters is cleaned. The return of dust from the hopper into the granulation chamber is controlled by a clocked sluice. The dust portions are returned into the fluidized behind a divertor plate in order to avoid its immediate elutriation. The flow rate of returned dust estimated as 250 g/3 s (0.0833 kg/s). This value can be confirmed by measuring the extinction of dust at the outlet (Grünewald, 2011). The granules are discharged continuously from the granulation chamber. The discharge rate is controlled by a rotary wheel sluice. After passing a sampling device leading to particle size analysis (*CAMSIZER, Retsch Technology*), the granules enter a "zigzag" classifier. The product granules of the desired particle size are collected and weighted. The remaining particles are pneumatically returned into the granulation chamber. The standard experimental conditions are listed in Table 1.

$\dot{M}_{fl}$	kg/h	75
$\dot{M}_{atom}$	kg/h	12
$\dot{M}_{class}$	kg/h	16
$\dot{M}_{susp}$	kg/h	4.3
x_{susp}	-	0.35
ϑ_{fl}	°C	180
ϑ_{atom}	°C	30
$\dot{M}_{nuc,ext}$	kg/h	0.1

Table 1: Standard experimental conditions for continuous operation

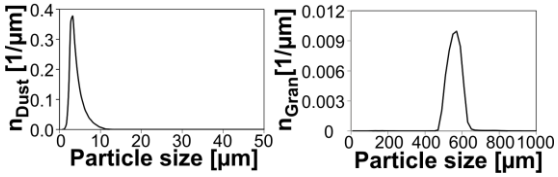

Figure 2: Initial particle size distribution of the dust (left) and the initial bed granules (right).

At the beginning of an experiment 1 kg of primary dust is stored in the filter. This dust is produced by spray drying of the suspension in the process without bed granules and has therefore the same PSD as the overspray. The external nuclei used in this experiment have the same distribution as the initial bed granules. The initial PSD of the dust and granules of are shown in Figure 2.

MODEL DESCRIPTION

Because of their different circulation times the dust phase and the granular phase are treated separately. The growth kinetics is obtained from the CFD simulation using the Direct Quadrature Method of Moments (DQMOM) (Fan et al., 2004). In this investigation the commercial CFD software *Fluent* is adopted and the relevant physical mechanisms are implemented therein.

Population balance of the granular phase

For the granular phase (d > 150 µm) macro agglomeration and breakage are negligible at these process conditions and they are therefore neglected in the simulation. Thus the PSD of the granules changes due to growth, which is caused by drop deposition and dust integration, and it changes due to inlet or outlet streams, namely the streams of nuclei originating from the dust phase (internal nuclei), of external nuclei and of withdrawn product granules. Hence, the population balance equation of the granules is written as:

$$\frac{\partial N_{Gran}(L)}{\partial t}+\frac{\partial\left(G_{L,Gran}\cdot N_{Gran}(L)\right)}{\partial L}=\dot{N}_{nuc,ext}+\dot{N}_{nuc,\mathrm{int}}-\dot{N}_{\mathrm{Pr}} \quad (1)$$

The growth rate $G_{L,Gran}$ is obtained from the CFD simulation using a simplified DQMOM (Li et al., 2011a) for a polydisperse system. The granules are described using two characteristic sizes with their respective weights. The rate of product withdrawal $\dot{N}_{\mathrm{Pr}}$ is derived from the rate passing through the rotary wheel $\dot{N}_{RWS}$ and a suitable classification function. $\dot{N}_{RWS}$ is deduced from the mass flow through the rotary wheel sluice $\dot{M}_{RWS}$ and the volume averaged size of granules d_{30}, which is easily obtained from the PSD of granules in the fluidized bed under the assumption that the granules are discharged representatively from the bed.

$$\dot{N}_{RWS}=\frac{\dot{M}_{RWS}}{\rho_{Gran}k_v d_{30}^3} \quad (2)$$

with k_v = π/6. In this experiment the flow rate through the rotary wheel sluice $\dot{M}_{RWS}$ is 9 kg/h. The classifier is described using a cumulative normal distribution function:

$$T(L)=\int_0^L\left(\frac{1}{\sqrt{2\pi}\cdot\sigma}\exp\left(-\frac{(L-\mu)^2}{2\sigma^2}\right)\right)dL \quad (3)$$

with σ = 110 µm and µ= 950 µm (Grünewald, 2011). The number rate of the external nuclei can be derived similarly using eq. 2 for a given PSD of external nuclei. The number of the internally formed nuclei is obtained from the population balance of the dust particles, i.e. the dust phase. The PBE of the granules is solved using a High Resolution Finite Volume Method (HRFVM) (Gunanwan et al., 2004).

Population balance of the dust phase

The particles constituting the dust phase not only grow due to collisions with drops but also due to agglomeration among themselves. This mechanism was proven by image analysis (Grünewald et al., 2010). Furthermore the number density of the dust phase changes due to overspray and dust integration as well as due to internal nucleation.

$$\frac{\partial N_{dust}(v)}{\partial t}+\frac{\partial\left(G_{v,dust,total}\cdot N_{dust}(v)\right)}{\partial V}= B_{agg}-D_{agg}-\dot{N}_{nuc,\mathrm{int}}+\dot{N}_{OS}-\dot{N}_{dust-\mathrm{int}} \quad (4)$$

The birth- and death-terms describing agglomeration are

$$B_{agg}=\left(\frac{1}{2}\int_0^V\beta_{total}n(V-V',t)n(V',t)dV'\right)dV \quad (5)$$

$$D_{agg}=\left(\int_0^\infty\beta_{total}n(V,t)n(V',t)dV'\right)dV\,, \quad (6)$$

with β_{total} being the collision frequency. The number rates of overspray $\dot{N}_{OS}$ and dust integration $\dot{N}_{dust-\mathrm{int}}$ as well as the collision frequency β_{total} and the growth rate of dust $G_{v,dust,total}$ are generated from the CFD simulation. To obtain the (internal) nucleation rate $\dot{N}_{nuc,\mathrm{int}}$ a lower size

limit of the granulate phases is defined by the smallest size of granules staying in the fluidized bed. As mentioned earlier, smaller particles than this cut size belong to the dust phase. This limit is about 150 µm at the given fluidization air flow and is calculated by equalling the superficial velocity of air in the granulation chamber and the terminal velocity of the granules. The Cell-Average Method (Kumar et al., 2006) is adopted to solve the PBE (eqn. 4) of the dust in this investigation.

Overall CFD simulation model

The rates, which are adopted in the population balance of the dust and in the population balance of the granules, are obtained from a six-phases CFD model (s. Figure 3).

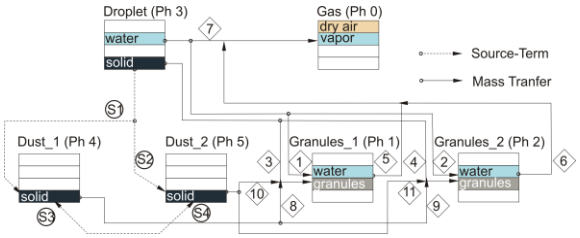

Figure 3: Mind-map of the overall model

The model contains one gas phase, one droplet phase, two granular phases and two dust phases. Each phase is composed of different species. In CFD the population balance equations of the two granular phases and the two dust phases are solved using DQMOM. The droplet phase comprises two species in this model, the solid and the water (liq.). For the following reason each granular phase also comprises two components, namely granules and water (liq.): The fraction of granular surface which is wetted by a liquid film must be considered in the simulation because the dust can only integrate on the wet surfaces of the granules. To calculate the spatial distribution of this fraction the evaporation rate of the liquid film must be evaluated. It depends on the temperature of the granules as well as on the local humidity and temperature of the air (Li et al., 2011b). The gas phase comprises dry air and vapor (water (g)). The evaporation of the water from the granules as well as from the droplets is formulated as mass transfers between phases by solving the respective mass and energy balances. The dust phases are simulated as compact solid and they have a density of solid (ρ_{solid} = 2700 kg/m^3). The granules are porous. Their density was measured and for simplicity reasons is assumed to be constant (ρ_{Gran} = 1700 kg/m^3). The accounted for inter-phasic mass transfers rates are listed in **Table 2**.

Number	From	To
1	Droplet/water	Granules_1/water
2	Droplet/water	Granules_2/water
3	Droplet/solid	Granules_1/Granules
4	Droplet/solid	Granules_2/Granules
5	Granules_1/water	Gas/vapor
6	Granules_2/water	Gas/vapor
7	Droplet/water	Gas/vapor
8	Dust_1/solid	Granules_1/Granules
9	Dust_1/solid	Granules_2/Granules
10	Dust_2/solid	Granules_1/Granules
11	Dust_2/solid	Granules_2/Granules

Table 2: Mass transfer rates between phases

The drop deposition rate and dust integration rate of the solid on both granular phases (stream numbers 3, 4 and 8-11) are modeled using an inertia deposition model (Li et al., 2011[a,b]). To quantify the growth rate of the dust particles (due to droplet deposition and due to dust agglomeration) their PBE must be solved in the CFD simulation. In this work the DQMOM with two nodes is adopted. The transport equations of the PSD of dust can be reduced to transport equations of the particle volume fractions and the particle sizes for two representative particle fractions (Nodes).

$$\frac{\partial \alpha_{s,i}}{\partial t} + \nabla\left(\vec{u}_i \alpha_{s,i}\right) = 3k_v L_i^2 b_i - 2k_v L_i^3 a_i \tag{7}$$

$$\frac{\partial \left(\alpha_{s,i} L_i\right)}{\partial t} + \nabla\left(\vec{u}_i \alpha_{s,i} L_i\right) = 4k_v L_i^3 b_i - 3k_v L_i^4 a_i \tag{8}$$

with phase index i = 1, 2. The right hand sides of the equations are the source terms for the volume fractions and the particle sizes. a_i and b_i are evaluated using a system of linear equations including the source terms of the k-th moments $\bar{S}_k$ of the dust phases.

$$(1-k)\sum_{i=1}^{N} L_i^k a_i + k\sum_{i=1}^{N} L_i^{k-1} b_i = \bar{S}_k \tag{9}$$

$\bar{S}_k$ is the result of birth, death (agglomeration) and of growth:

$$\bar{S}_k = \left(\bar{B}_{agg,k} - \bar{D}_{agg,k}\right) + Growth \tag{10}$$

$$\bar{B}_{agg,k} = \frac{1}{2}\sum_{i=1}^{N} w_i \sum_{j=1}^{N} w_j \left(L_i^3 + L_j^3\right)^{k/3} \beta\left(L_i, L_j\right) \tag{11}$$

$$\bar{D}_{agg,k} = \frac{1}{2}\sum_{i=1}^{N} L_i^k w_i \sum_{j=1}^{N} w_j \beta\left(L_i, L_j\right) \tag{12}$$

$$Growth = \sum_{i=1}^{N} k \cdot w_i L_i^{k-1} G\left(L_i\right) \tag{13}$$

The collision rate $\beta\left(L_i, L_j\right)$ is modeled using the turbulence shear model proposed by Saffman (1956):

$$\beta\left(L_i, L_j\right) = \sqrt{8\pi} r^2 \left(\begin{array}{l} \left(\frac{1}{9} r^2 \frac{\varepsilon}{\nu} \right. \\ \left. + \left(\tau_i - \tau_j\right)^2 \left\langle \left(\frac{Du}{Dt}\right)^2 \right\rangle \right)^{1/2} \\ \left. + \frac{1}{3}\left(\tau_i - \tau_j\right)^2 g^2 \right) \end{array} + u_{rel,i,j} \right) \tag{14}$$

with the cross-sectional radius r

$$r = \frac{L_i + L_j}{2} \tag{15}$$

the energy dissipation rate ε, and the kinematic viscosity ν. Following Batchelor (1951) for large Reynolds numbers

$$\left\langle \left(\frac{Du}{Dt}\right)^2 \right\rangle = 1{,}3 \frac{\varepsilon^{3/2}}{\nu^{1/2}}. \tag{16}$$

The relaxation time τ_i is defined by

$$\tau_i = \frac{\rho_P L_i^2}{36 \mu_g}. \tag{17}$$

It is assumed that every collision is successful. After the collision the two particles adhere to each other and the collision rate is then equal to the agglomeration rate. Growth of the dust is due to the collision between dust particles and droplets. In case the number concentration of the dust phase i in a cell is $N_{conc,i}$ and the number

concentration of droplets in a cell is $N_{conc,drop,}$ then the collision rate $\dot{N}_{coll}$ between them is

$$\dot{N}_{coll} = \beta_{i,drop} N_{conc,i} N_{conc,drop} \,. \tag{18}$$

Whereas $\beta_{i,drop}$ is calculated from Eq. (14). After a time step Δt the new particle size due to collision:

$$L_i^{t+\Delta t} = \left(\frac{N_i \left(L_i^t\right)^3 + \frac{\dot{N}_{coll} \cdot d_{drop}^3 \cdot x_{drop} \cdot \rho_{drop}}{\rho_{solid}} \Delta t}{N_i} \right)^{1/3} \tag{19}$$

Thus, the growth rate in this time step for the dust phase i is:

$$G\left(L_i\right) = \frac{L_i^{t+\Delta t} - L_i^t}{\Delta t} \tag{20}$$

The thus generated growth and agglomeration rates of dust are averaged over the simulation time and applied to the PBE of the dust to obtain the evolution of the PSD for a long process time. Thus we use a simple assumption that for each of both dust phases the agglomeration rate and the growth rate are size-independent. Therefore we can easily obtain the agglomeration rate from the temporal change of the zeroth moment m_0 (total number) of the dust (Bramley et al., 1996):

$$\frac{dm_0}{dt} = -\frac{1}{2} \beta_{total} m_0^2 \tag{21}$$

and the total growth rate $G_{L,dust,total}$ is calculated from the temporal change of the third moment m_3:

$$\frac{dm_3}{dt} = \frac{6}{\pi} \frac{\dot{m}_{s,drop-dust}}{\rho_{solid}} = 3 G_{L,dust,total} \frac{A_{dust}}{\pi} \tag{22}$$

with A_{dust} being the total dust area and $\dot{m}_{s,drop-dust}$ the solid mass flow due to collisions between drops and dust. The growth rate is deduced:

$$G_{L,dust,total} = \frac{2}{\rho_{solid} A_{dust}} \dot{m}_{s,drop-dust} \tag{23}$$

$$G_{v,dust,total} = G_{L,dust,total} \cdot \frac{\pi}{2} L^2 \tag{24}$$

Procedure of the simulation

The following simulation procedure is adopted (s. Figure 4): From the initial PSD and bed mass two granular phases are generated with their respective diameters and masses by applying the product difference method (Marchisio et al., 2003) to the first four moments of the initial PSD. Then, fluid dynamics of the three-phasic system (gas phase, two granular phases) is solved until rather constant conditions are attained (~10 s process time, time step by 10^{-4} s). A 2D axis-symmetrical Grid (cell number 9800) is used to solve the fluid dynamics. The models of Gidaspow (1994) and Syamlal (1987) are adopted to model the drag between the gas and the granules and the drag between the two granular phases. Thereafter, the droplet phase is injected as the fourth phase to solve the temperature field in the granulation chamber. Note, for this calculation the solids in the droplets are neglected, and only water is injected. Nevertheless, the two dust phases are established as fifth and sixth phase, but at this stage their respective mass flux is 0. About 20 s of process time have to be simulated before the average temperature of the granules reaches steady state. Then the two dust phases, which are also generated from a given initial mass and size distribution, are fed to the bottom of the granulation chamber. The droplet is at this stage changed from water to suspension composed of solid and water and the entire granulation process with all mechanisms is simulated (time step by 10^{-5} s, CPU time for one CFD kinetic updating is about 2 weeks.).

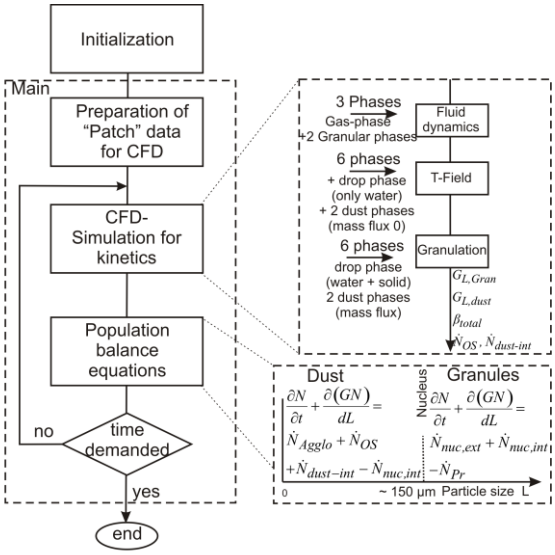

Figure 4: Procedure of the Simulation

The thus obtained kinetics for the granule and dust phases are applied in their respective PBEs to solve for the development of their PSD for a given time interval (The simulation time at this stage takes about 40 s for 30 minutes process time.). Thereafter, the kinetics needs to be updated by a new CFD simulation. The new generated PSDs and masses of granules and dust are used as the initial data for the next iteration until the end of the simulation time.

RESULTS

In this investigation the standard granulation process (see Tab. 1) is simulated for 300 minutes with the kinetics being updated every 30 minutes. The node data for every update are listed in **Table 3**.

Time [min.]	L_1 [mm]	L_2 [mm]	w_1 [-]	w_2 [-]
0	0.493	0.589	0.321	0.679
30	0.634	0.785	0.515	0.485
60	0.593	0.812	0.293	0.707
90	0.634	0.868	0.462	0.538
120	0.440	0.843	0.208	0.792
150	0.352	0.855	0.214	0.786
180	0.380	0.837	0.278	0.722
210	0.382	0.856	0.338	0.662
240	0.338	0.876	0.501	0.499
270	0.308	0.924	0.397	0.603

Table 3: *Used weights and abscissa at each update of the kinetics*

As an example, the simulated results at 90 minutes process time are discussed. In this simulation the temperature field is simulated until 35 s process time. After that one fourth of the total dust is given at the boundary into the process to simulate the drop deposition, dust integration and nucleation for one dust-cycle, namely the time between each jet-cleaning (30 s here). Figure 5 depicts the mass flow rates of solid onto the granular phase due to drop deposition. At the beginning the dust needs about 0.6 s to

travel through the bed and arrive at the jet, thus no dust is colliding with the droplets during that period. The drop deposition increases fast from 0 to the maximum. Then it decreases dramatically because the collisions of the drops with dust particles happen concurrently. After 3.6 s the drop deposition increases again to the maximum as before.

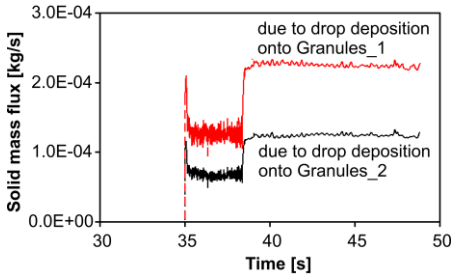

Figure 5: Mass flow rates on each granular phase due to drop deposition ($\dot{m}_{drop-dep,1}$, $\dot{m}_{drop-dep,2}$)

Figure 6 shows the dust integration rates from each dust phase to each granular phase $\dot{m}_{dust-\mathrm{int},i,j}$ (j,i = 1,2, the index of dust phases and granular phases). Due to the discontinuous dust feeding the dust integration happens only for a few seconds and then tends to zero. The growth rate of each node is then

$$G_{V,Gran,i} = \frac{dV_{Gran,i}}{dt} = \frac{\dot{m}_{drop-dep,i} + \dot{m}_{dust-\mathrm{int},1,i} + \dot{m}_{dust-\mathrm{int},2,i}}{N_i \rho_{Gran}} = \frac{d\left(k_v L_i^3\right)}{dt} = \frac{\pi}{2} L_i^2 \frac{dL_i}{dt} = \frac{\pi}{2} L_i^2 G_{L,Gran,i} \quad (25)$$

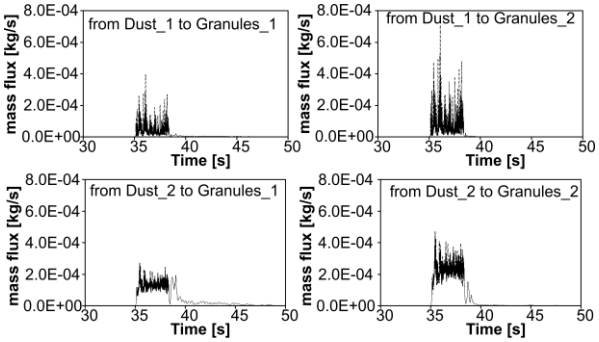

Figure 6: Mass flow rates of the dust integration ($\dot{m}_{dust-\mathrm{int},1,1}$, $\dot{m}_{dust-\mathrm{int},1,2}$, $\dot{m}_{dust-\mathrm{int},2,1}$, $\dot{m}_{dust-\mathrm{int},2,2}$)

The number of granules of each granular phase is obtained from the mass M_i and the abscissa L_i

$$N_i = \frac{M_i}{\rho_{solid}\left(k_v L_i^3\right)} = \frac{M_{bed} \cdot w_i L_i^3 / \left(\sum_{j=1}^{N} w_j L_j^3\right)}{\rho_{solid}\left(k_v L_i^3\right)} \quad (26)$$

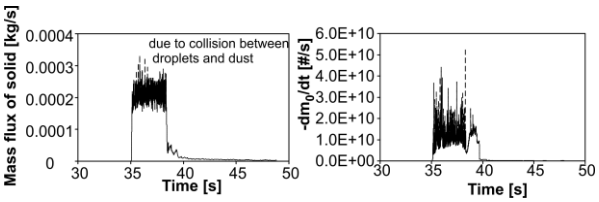

Figure 7: Total solid mass flow rate due to collision between droplets and dust (left) and temporal change of the first moment of the dust phase (right)

To obtain average growth rates all streams of drop deposition and dust integration are averaged by the time interval of jet-cleaning (30 s). Figure 7 (left) shows the total mass flow rate of the solid due to the collisions between dust and droplets. This value is used in eq. 22. The temporal change of the particle number used in eq. 21 is also shown in Figure 7 (right). In Table 4 the calculated agglomeration rate β_{total} (s. eq. 21) and growth rate $G_{L,dust,total}$ are given for each update. The dust size distribution is given versus process time in Figure 8. At first the dust coarsens because of agglomeration between the dust particles.

Time [min.]	β_{total} [1/s]	$G_{L,dust,total}$ [m/s]	Mass [kg]
0	1.34E-16	9.22E-11	1.000
60	3.16E-16	9.49E-11	1.101
90	1.79E-15	8.17E-11	1.072
120	1.53E-14	1.21E-10	0.994
150	2.63E-14	1.73E-10	0.862
180	1.06E-13	1.47E-10	0.734
210	2.56E-13	1.73E-10	0.658
240	2.21E-14	3.68E-10	0.448
270	1.19E-14	2.84E-10	0.493
300			0.489

Table 4: Simulated growth and agglomeration rate of dust

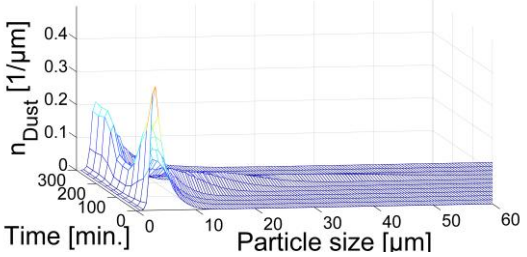

Figure 8: Simulated PSD of dust over the process time

Later on the dust size distribution changes due to newly formed dust from overspray. It is strongly influenced by the bed mass. The evolution of the bed mass is shown in Figure 9. It increases steeply during the first 60 minutes because the granules grow, however they are not large enough to be discharged by the classifier. Thereafter the mass of the bed decreases dramatically due to the discharging of the product. The mass flow of the product decreases because the initial bed granules are almost discharged and the production is governed by the growing external and internal nuclei. Increasing the bed mass enhances the drop deposition on the granules, i.e. it inhibits overspray. After about 100 minutes the median of the size distribution moves back to small particle sizes because the bed mass decreases due to removal product and consequently overspray increases.

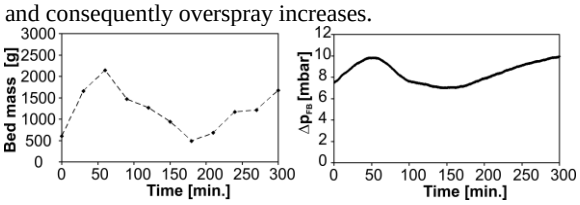

Figure 9 Simulated bed mass and the experimental pressure drop over the process time

Further, more internal nuclei are formed since the dust slowly becomes coarser. Fig. 10 shows clearly the coarsening of the dust particles at the end of the process by 300 minutes process time. These small nuclei need a long residence time in the fluidized bed to grow and become (product) granules. Thus, the bed mass slowly

increases again. In the employed experimental configuration it is not possible to measure the bed mass during the process. The accessible measurement parameter, which can confirm the changing of the bed mass indirectly, is the pressure drop of the fluidized bed. Its development over the process time is also shown in Figure 9 (right). The tendency of the simulated development of the bed mass fits to the measured pressure drop.

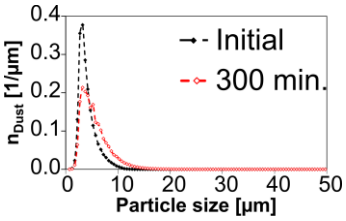

Figure 10: Simulated dust size distributions at the beginning and at the end of the process

It was found from the experiment that the sample of bed granules by this experimental configuration is representative only for the particles larger than 330 µm, thus both of the PSDs from experiments and simulations are cut under 330 µm.

The comparison of the PSD qualitatively shows the agreement between the experiment and simulation. Figure 11 shows the detailed comparison at a particular process time. Generally the simulated data agree well with the experimental ones. At the end of the process the simulated first peak of the granules, which identifies the internal nuclei (external nuclei have a size about 500-600 µm) is lower than the experimental one. It reveals that the simulated number-flow of the internal formed nuclei is lower than the experimental one. It is assumed, that the difference between the simulated and the experimental PSDs is due to the following reasons. Firstly, the dust is returned at the perforated bottom in the simulation. In the experiment the dust is returned behind a divertor plate into the fluidized bed. It leads to a deviation of the simulation to the reality. Secondly, the lower size limit of the granules is estimated using the terminal velocity at the given operating conditions. The change of this limit has an influence on the newly formed nuclei and further on the PSD of the granules. Furthermore the mass flow rate of granules through the wheel sluice is assumed to be constant in the simulation. In fact and in the practice, it depends on the bed mass. Certainly, this fact has also influence on the separation behavior of the classifier.

CONCLUSION

In this investigation a multi-scale simulation using a combination of CFD and PBE is adopted to describe a continuously operated fluidized bed spray granulation process. The growth kinetics of the granules and of the dust are generated from the CFD simulation for short process times, in which the process relevant mechanisms, like drop deposition, drying, dust integration and internal nucleation, are implemented, and applied into 1-dimensional PBEs of the particle for long process times. The DQMOM is adopted in the CFD simulation to solve the PBE for the dust particles. A continuous process is simulated for 300 minutes process time using 9 kinetics update runs (every 30 minutes). The simulated timely developments of the PSD and of the bed mass agree well with the experimental ones.

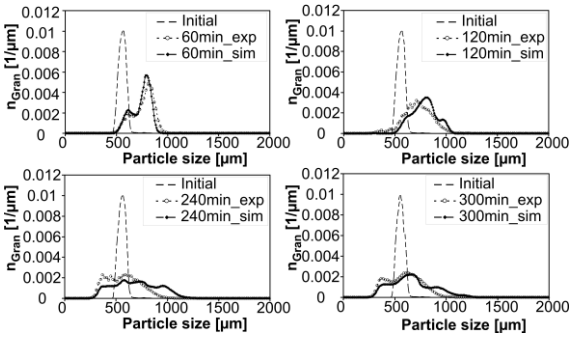

Figure 11: Simulated and experimental particle size distributions at particular process time

ACKNOWLEDGEMENTS

The authors thank the BASF SE, Ludwigshafen Germany for providing the financial and scientific support.

REFERENCES

BATCHELOR, G.K. (1951), Pressure Fluctuations in Isotropic Turbulence, *Proc. Camb. Phil. Soc*, **47**, 359-374

BRAMLEY, A.S., HOUNSLOW M. and R.L. RYALL (1996), Aggregation during Precipitation from Solution: A Method for Extracting Rates from Experimental Data, *J. Colloid Interface Sci.*, **184**, 155-165

FAN, R., MARCHISIO, D.L. and R.O. FOX (2004), Application of the Direct Quadrature Method of Moments to Polydisperse Gas-Solid Fluidized Bed, *Powder Technol.*, **139**, 7-20

GIDASPOW, D. (1994), Multiphase Flow and Fluidization: Continuum and Kinetic Theory Description, Academic Press, New York

GRÜNEWALD, G., WESTHOFF, B. and M. KIND (2010), Fluidized Bed Spray Granulation: Nucleation Studies with Steady-State Experiments, *Drying Technol.*, **28**, 349-360

GRÜNEWALD, G. (2011), Staubeinbindung und Keimbildung bei der Wirbelschicht-Sprühgranulation, Dissertation, Cuvillier, Göttingen

GUNAWAN, R., FUSMAN, I. and R.D. BRAATZ (2004), High Resolution Algorithms for Multidimensional Population Balance Equations, *AIChE J.*, **50**, 2738-2749

KUMAR, J., PEGLOW, M., WARNECKE, G., HEINRICH, S. and L. MÖRL (2006), Improved accuracy and convergence of discretized population balance for aggregation: The cell average technique, *Chem. Eng. Sci.*, **61**, 3327-3342

LI, Z., KIND, M. and G. GRÜNEWALD (2011a), Modeling the Growth Kinetics of Fluidized Bed Spray Granulation, *Chem. Eng. Technol.*, **34**, 1067-1075

LI, Z., KESSEL, J., GRÜNEWALD, G. and M., KIND (2011b), CFD Simulation on drying and dust integration in fluidized bed spray granulation, Proceedings of 7th Asia-Pacific Drying Conference, Tianjin, China.

MARCHISIO, D.L., PIKTURNA, J.T., FOX, R.O., VIGIL, R.D. and A.A. BARRESI (2003), Quadrature Method of Moments for Population-Balance Equations, *AIChE J.*, **49**, 1266-1276

SAFFMAN, P.G. and J.S. TURNER (1956), On the collision of drops in turbulent clouds, *J. Fluid Mech.*, **1**, 16-30.

SYAMLAL, M. (1987), The Particle-Particle Drag Term in a Multiparticle Model of Fluidization, National Technical Information Service, Springfield, VA, DOE/MC/21353-2373